

**LA-UR-22-23793**

Accepted Manuscript

## Origin of Plutonium-244 in the Early Solar System

Lugaro, Maria  
Yague Lopez, Andres  
Soós, Benjámín  
Cote, Benoit  
Pet , Maria K.  
Vassh, Nicole  
Wehmeyer, Benjamin  
Pignatari, Marco

Provided by the author(s) and the Los Alamos National Laboratory (2022-08-04).

**To be published in:** Universe

**DOI to publisher's version:** 10.3390/universe8070343

**Permalink to record:**

<http://permalink.lanl.gov/object/view?what=info:lanl-repo/lareport/LA-UR-22-23793>



Los Alamos National Laboratory, an affirmative action/equal opportunity employer, is operated by Triad National Security, LLC for the National Nuclear Security Administration of U.S. Department of Energy under contract 89233218CNA000001. By approving this article, the publisher recognizes that the U.S. Government retains nonexclusive, royalty-free license to publish or reproduce the published form of this contribution, or to allow others to do so, for U.S. Government purposes. Los Alamos National Laboratory requests that the publisher identify this article as work performed under the auspices of the U.S. Department of Energy. Los Alamos National Laboratory strongly supports academic freedom and a researcher's right to publish; as an institution, however, the Laboratory does not endorse the viewpoint of a publication or guarantee its technical correctness.

Article

# Origin of Plutonium-244 in the Early Solar System

Maria Lugaro<sup>1,2,3,4,\*</sup> , Andrés Yagüe López<sup>5,†</sup> , Benjámín Soós<sup>1,2,3</sup>, Benoit Côté<sup>1,2,6,7,†</sup> , Mária Pető<sup>1,2</sup> , Nicole Vassh<sup>8</sup>, Benjamin Wehmeyer<sup>1,2,9</sup> and Marco Pignatari<sup>1,2,6,10,†</sup>

- <sup>1</sup> Konkoly Observatory, Research Centre for Astronomy and Earth Sciences (CSFK), Eötvös Loránd Research Network (ELKH), Konkoly Thege Miklós út 15-17, 1121 Budapest, Hungary; soos.benjamin@csfk.org (B.S.); benoit.cote@csfk.org (B.C.); maria.k.peto@gmail.com (M.P.); benjamin.wehmeyer@csfk.org (B.W.); marco.pignatari@csfk.org (M.P.)
- <sup>2</sup> CSFK, MTA Centre of Excellence, Konkoly Thege Miklós út 15-17, 1121 Budapest, Hungary
- <sup>3</sup> Institute of Physics, ELTE Eötvös Loránd University, Pázmány Péter Sétány 1/A, 1117 Budapest, Hungary
- <sup>4</sup> School of Physics and Astronomy, Monash University, Melbourne, VIC 3800, Australia
- <sup>5</sup> Computer, Computational and Statistical Sciences (CCS) Division, Center for Theoretical Astrophysics, Los Alamos National Laboratory, Los Alamos, NM 87545, USA; ayaguelopez@lanl.gov
- <sup>6</sup> Joint Institute for Nuclear Astrophysics—Center for the Evolution of the Elements (JINA-CEE), USA
- <sup>7</sup> Department of Physics and Astronomy, University of Victoria, Victoria, BC V8P 5C2, Canada
- <sup>8</sup> TRIUMF, 4004 Wesbrook Mall, Vancouver, BC V6T 2A3, Canada; nvassh@gmail.com
- <sup>9</sup> Centre for Astrophysics Research, University of Hertfordshire, College Lane, Hertfordshire AL10 9AB, UK
- <sup>10</sup> Milne Centre for Astrophysics, University of Hull, Hull HU6 7RX, UK
- \* Correspondence: maria.lugaro@csfk.org
- † NuGrid Collaboration, <http://nugridstars.org>.

**Abstract:** We investigate the origin in the early Solar System of the short-lived radionuclide <sup>244</sup>Pu (with a half life of 80 Myr) produced by the *rapid* (*r*) neutron-capture process. We consider two large sets of *r*-process nucleosynthesis models and analyse if the origin of <sup>244</sup>Pu in the ESS is consistent with that of the other *r* and *slow* (*s*) neutron-capture process radioactive nuclei. Uncertainties on the *r*-process models come from both the nuclear physics input and the astrophysical site. The former strongly affects the ratios of isotopes of close mass (<sup>129</sup>I/<sup>127</sup>I, <sup>244</sup>Pu/<sup>238</sup>U, and <sup>247</sup>Pu/<sup>235</sup>U). The <sup>129</sup>I/<sup>247</sup>Cm ratio, instead, which involves isotopes of a very different mass, is much more variable than those listed above and is more affected by the physics of the astrophysical site. We consider possible scenarios for the evolution of the abundances of these radioactive nuclei in the galactic interstellar medium and verify under which scenarios and conditions solutions can be found for the origin of <sup>244</sup>Pu that are consistent with the origin of the other isotopes. Solutions are generally found for all the possible different regimes controlled by the interval ( $\delta$ ) between additions from the source to the parcel of interstellar medium gas that ended up in the Solar System, relative to decay timescales. If *r*-process ejecta in interstellar medium are mixed within a relatively small area (leading to a long  $\delta$ ), we derive that the last event that explains the <sup>129</sup>I and <sup>247</sup>Cm abundances in the early Solar System can also account for the abundance of <sup>244</sup>Pu. Due to its longer half life, however, <sup>244</sup>Pu may have originated from a few events instead of one only. If *r*-process ejecta in interstellar medium are mixed within a relatively large area (leading to a short  $\delta$ ), we derive that the time elapsed from the formation of the molecular cloud to the formation of the Sun was 9–16 Myr.

**Keywords:** short-lived radioactivity; early Solar System; rapid neutron captures; galactic chemical evolution



**Citation:** Lugaro, M.; Yagüe López, A.; Soós, B.; Côté, B.; Pető, M.; Vassh, N.; Wehmeyer, B.; Pignatari, M. Origin of Plutonium-244 in the Early Solar System. *Universe* **2022**, *8*, 343. <https://doi.org/10.3390/universe8070343>

Academic Editor: Marcello Abbrescia

Received: 29 April 2022

Accepted: 16 June 2022

Published: 22 June 2022

**Publisher's Note:** MDPI stays neutral with regard to jurisdictional claims in published maps and institutional affiliations.



**Copyright:** © 2022 by the authors. Licensee MDPI, Basel, Switzerland. This article is an open access article distributed under the terms and conditions of the Creative Commons Attribution (CC BY) license (<https://creativecommons.org/licenses/by/4.0/>).

## 1. Introduction

There are 17 short-lived radioactive (SLR, with half lives of the order of 0.1 to 100 Myr) nuclei known to have been (or potentially have been) present in the early Solar System (ESS) [1]. Three of them, <sup>129</sup>I, <sup>244</sup>Pu, and <sup>247</sup>Cm, have the specific property to be produced in the Galaxy almost exclusively by the process of *rapid* neutron captures (the *r* process). Among those three, live <sup>244</sup>Pu from the present-time interstellar medium has also been

detected in young sediments of the ocean floor [2,3]. Furthermore,  $^{244}\text{Pu}$  and  $^{247}\text{Cm}$  are actinides located beyond Pb and Bi at mass numbers around 208–210, the end point of the *slow* neutron-capture (*s*) process [4]. Therefore, they are exclusively of *r*-process origin. Being located beyond the classical third *r*-process peak at Pt and Au, actinides are typically produced if the number of neutrons per seed is relatively large. Instead,  $^{129}\text{I}$  belongs to the classical second *r*-process peak. It has only a very minor (a few percent) contribution from the *s* process because the unstable isotope that precedes it on the *s*-process path,  $^{128}\text{I}$ , has a half life of 25 min only and decays faster than the typical time required for capturing a neutron. These three *r*-process isotopes have most likely the same *r*-process origin (as indicated by elemental abundance observed in halo stars, [5]). They can be studied individually or together to provide evidence on the history of the material that made up the Solar System [6] and to set constraints on the *r*-process astrophysical site and its nuclear input, which are both extremely uncertain [7–10]. In particular, Côté et al. [8] (hereafter Paper I) constrained the last *r*-process source to have contributed to the solar material by comparing the  $^{129}\text{I}/^{247}\text{Cm}$  ratio observed in primitive meteorites to nucleosynthesis calculations based on neutron star (NS-NS) merger, black hole–neutron star (NS-BH) merger, and magneto-rotational supernova simulations. Here, we extend that study to  $^{244}\text{Pu}$ , to investigate if it is possible to find an explanation for the presence of this SLR isotope in the ESS compatible with the explanation for the presence of the other SLR isotopes heavier than iron, also well known to have been present in the ESS.

Table 1 summarises the main properties and information available on the four isotopic ratios under consideration here:  $^{129}\text{I}/^{127}\text{I}$ ,  $^{244}\text{Pu}/^{238}\text{U}$ ,  $^{247}\text{Cm}/^{235}\text{U}$ , and  $^{129}\text{I}/^{247}\text{Cm}$ . We only analyse isotopic ratios because the most direct evidence that comes from the analysis of meteoritic material on ESS values is not absolute abundances, but abundance values relative to each other. Absolute abundances suffer from many uncertainties, e.g., chemical separation in the nebula, in the meteorite parent body, and/or during chemical analysis, as well as dilution from the original stellar source. The ratios of interest are those of each estimated SLR abundance relative to a long-lived or a stable isotope. These ratios are directly measured in primitive meteorites and their components (the first three rows of Table 1), or derived from the ratios directly measured (last row), as in the case of the  $^{129}\text{I}/^{247}\text{Cm}$  ratio. This last ratio provides us with a further observational constraint because  $^{129}\text{I}$  and  $^{247}\text{Cm}$  have very similar half lives [11]<sup>1</sup>. This allowed to remove several theoretical uncertainties in Paper I, providing a direct window into the astrophysical conditions of the *r*-process site that produced the  $^{129}\text{I}$  and  $^{247}\text{Cm}$  in the ESS. Note that, instead, it is not possible to extract any further meaningful constraints from the  $^{129}\text{I}/^{244}\text{Pu}$  and  $^{247}\text{Cm}/^{244}\text{Pu}$  ratios because their half lives are very different from each other [11].

**Table 1.** Properties of the three ratios that involve SLR nuclei of *r*-process origin that were present in the ESS: the mean lives of the isotopes at numerator, at denominator, and of their ratio ( $\tau_{\text{num}}$ ,  $\tau_{\text{den}}$ , and  $\tau_{\text{ratio}} = \tau_{\text{num}} \times \tau_{\text{den}} / (\tau_{\text{num}} - \tau_{\text{den}})$ , respectively, all in Myr), and the ESS values (at  $2\sigma$ , from [1]). We also show, in the last column, the three values of the *K* factor that affect each of the ratios when predicted by the GCE model. This factor accounts for the star formation history and efficiency, the star-to-gas mass ratio, and the galactic outflows (Section 3). The uncertainties on these quantities result in a minimum ( $K_{\text{min}}$ ), a best-fit ( $K_{\text{best}}$ ), and a maximum ( $K_{\text{max}}$ ) value of each ratio.

Ratio	$\tau_{\text{num}}$	$\tau_{\text{den}}$	$\tau_{\text{ratio}}$	ESS Ratio	$K_{\text{min}}, K_{\text{best}}, K_{\text{max}}$
$^{129}\text{I}/^{127}\text{I}$	22.6	stable	22.6	$(1.28 \pm 0.03) \times 10^{-4}$	1.6, 2.3, 5.7
$^{244}\text{Pu}/^{238}\text{U}$	115	6447	117	$(7 \pm 2) \times 10^{-3}$	1.5, 1.9, 4.1
$^{247}\text{Cm}/^{235}\text{U}$	22.5	1016	23.0	$(5.6 \pm 0.3) \times 10^{-5}$	1.1, 1.2, 1.8 <sup>b</sup>
$^{129}\text{I}/^{247}\text{Cm}$	22.6	22.5	270 <sup>a</sup> (100–3000)	438 ± 184	1, 1, 1

<sup>a</sup> Values taken from the asymmetric  $\tau_{\text{ratio}}$  distribution shown in Figure S4 of Paper I. The first value is roughly the peak of the distribution, and the values in parenthesis represent most of its total range. <sup>b</sup> Values corrected relative to those reported in Paper I.

Out of the four ratios reported in Table 1,  $^{244}\text{Pu}/^{238}\text{U}$  has not been considered yet within a global analysis of origin of the SLR nuclei heavier than iron in the ESS. This is for two main reasons: first, its half life of 80 Myr is very different from that of the other two isotopes of roughly 15 Myr, therefore, the modelling of its abundance in the interstellar medium (ISM) is likely to present a different behaviour (see discussion in Section 3). Second, its ESS abundance is less certain than those of the other two isotopes. The ESS  $^{129}\text{I}/^{127}\text{I}$  ratio has an uncertainty of roughly 2% at  $2\sigma$  and many studies agree on its value, suggesting that systematic uncertainties are not significant [12]. The  $^{247}\text{Cm}/^{235}\text{U}$  was established with an uncertainty of roughly 6% at  $2\sigma$  thanks to the discovery of the special meteoritic inclusion, named Curious Marie, rich in U [13]. More data on different samples is still needed to completely establish this value.

In the case of the ESS  $^{244}\text{Pu}$  abundance (i.e., the  $^{244}\text{Pu}/^{238}\text{U}$  ratio), instead, not only is the uncertainty for the value reported in Table 1 roughly 30%, but also there are potential systematic uncertainties in the determination of the ESS value. The ESS  $^{244}\text{Pu}$  abundance can be estimated by xenon isotope studies of meteorites, since  $^{129}\text{Xe}$  and the heavy  $^{131-136}\text{Xe}$  are stable isotopes produced by the spontaneous fission of  $^{244}\text{Pu}$ . Moreover, solids are extremely poor in noble gases and the radiogenic and fissionogenic xenon signatures may become significant over time and, hence, can be quantified at high precision. Studies have been focusing on gas-poor meteoritic materials: mineral separates [14]; CAIs [15,16]; differentiated meteorites with simple cooling histories, such as angrites [17] and eucrites [18]; and high-metamorphic-grade ordinary chondrites [19]. Currently, there are two “best estimates” of ESS using different approaches. Lugmair and Marti [17] normalized  $^{244}\text{Pu}$  to  $^{150}\text{Nd}$ , an *r*-process-only isotope of Nd, because they found an achondrite (Angra dos Reis) where they could prove that the geochemical analogue of Pu is Nd, and potential modification of the Pu/Nd ratio with respect to the Solar System abundances can be ruled out. They reported  $^{244}\text{Pu}/^{238}\text{U}$  ratios  $\simeq 0.0043$  at the adjusted time of Solar-System formation [20]. The value reported in Table 1 (0.007) is a different estimate by [19], who used a different approach. As the fissionogenic signature is dominated by  $^{244}\text{Pu}$ -derived xenon in meteorites, they irradiated an exceptionally gas-poor ordinary chondrite (St Severin) with thermal neutrons to induce the fission of  $^{235}\text{U}$  and derived the  $^{244}\text{Pu}/^{238}\text{U}$  ratio from the component analysis of xenon isotope measurements alone. This value is almost twice as high as the value provided by the Angra dos Reis study, and it is in better agreement with the more recent analysis of Xe in ancient terrestrial zircons from Western Australia [21]. In summary, the major challenge is to find a meteorite sample that is representative of the Solar System, and for which geochemical processes that could potentially modify the relative abundances of Pu to U or rare earth elements with respect to the chondritic composition is well-understood, and the effect can be corrected for. Here, we will consider for the ESS  $^{244}\text{Pu}/^{238}\text{U}$  ratio the value reported in Table 1. If the “true” value was eventually found to be lower, for example, by a factor of two, all the times calculated and reported in our analysis below would have to be increased by 80 Myr.

The aim of this paper is to investigate possible self-consistent solutions for the origin of the abundances of all the SLR nuclei heavier than iron observed to have been present in the ESS, including  $^{244}\text{Pu}$ . These observed abundances are represented by the four *r*-process ratios reported in Table 1, as well as the SLR isotopes produced by *slow* neutron captures (the *s* process, specifically  $^{107}\text{Pd}$ ,  $^{135}\text{Cs}$ , and  $^{182}\text{Hf}$ , as discussed in [22]). We start by discussing predictions from state-of-the-art models of the *r* process for the three SLR nuclei of interest and their reference isotopes (Section 2). Then, in Section 3, we consider the temporal evolution of the  $^{244}\text{Pu}/^{238}\text{U}$  ratio in the ISM and discuss if there are solutions for its ESS value that are consistent with the abundances of the other SLR nuclei heavier than iron. Finally, in Section 4, we present our summary, conclusions, and suggestions for future work.

## 2. Nucleosynthesis Calculations

We consider the large set of *r*-process abundances published with Paper I and calculated with the nuclear network code WINNET<sup>2</sup> [23,24] and the nucleosynthesis network PRISM<sup>3</sup> [25,26]. All the abundances reported and used in this work, are taken at 1 Myr after the nucleosynthetic event, i.e., they are not decayed completely, given that we are interested in SLR nuclei.

Table 2 lists all the WINNET models considered here and the relationship between the labels used in Paper I and the shorter labels used here. The sites and the nuclear physics sets, with all their relevant references, are described in detail in Paper I and Ref. [27]. Here, we remind briefly that the nomenclature of the nuclear input is as follows: [D,J,Jm] denotes the mass model (D for Duflo Zuker, J for JINA reaclib, Jm for JINA with Marketin theoretical  $\beta$  decays). The “h” indicates that the nuclear heating subroutine was turned on [28]), modifying the temperature evolution of the trajectory. Finally, [f1,f2,f4] represent three different fission fragment models. There are, in total, 3 (top)  $\times$  3 (bottom) nuclear labels, i.e., nine sets of nuclear inputs (right side of the table), and seven astrophysical sites (left side of the table), therefore, a total of 63 WINNET models. The tabulated abundances of the six isotopes of interest here (together with the Eu isotopes and <sup>232</sup>Th for future reference) can be found in Supplementary Table S1.

**Table 2.** The correspondence of the astrophysical site and nuclear input labels are used here to indicate the WINNET models and those used in Paper I, where a full description of each site and nuclear model and relevant references can also be found. The total mass ejected by each site is also indicated.

Site Label	Site Label (Paper I)	Mass Ejected (M <sub>⊙</sub> )	Nuclear Label	Nuclear Label (Paper I)
R1010	NS-NS merger dyn. ejecta (R)	$7.64 \times 10^{-3}$	Dhf	DZ10
R1450	NS-BH merger dyn. ejecta (R)	$2.38 \times 10^{-2}$	Jhf	FRDM
Bs125	NS-NS merger dyn. ejecta (B)	$5.50 \times 10^{-4}$	Jmhf	FRDM(D3C*)
FMdef	NS-NS merger disk ejecta 1	$1.70 \times 10^{-3}$	1	Panov
FMs6	NS-NS merger disk ejecta 2	$1.27 \times 10^{-3}$	2	K & T
FMv0.10	NS-NS merger disk ejecta 3	$4.06 \times 10^{-3}$	4	ABLA07
Wmhd	MR SN	$6.72 \times 10^{-3}$		

In the case of the PRISM models, the nomenclature is identical to that used in Paper I (Table S3), and references therein. In this case, four sites are considered (the dynamical ejecta of two NS–NS mergers and two NS–BH models), and combined with ten different mass models, of which four are also investigated using alternative  $\beta$  decays (the “Mkt” label, here, corresponding to the “D3C\*” label in Paper I). The total is, therefore,  $4 \times 14 = 56$  PRISM models. The tabulated ratios of interest here can be found in Supplementary Table S2.

The four ratios of interest from all the models are plotted in Figures 1 and 2. As expected, ratios of isotopes of similar mass (Figure 2) are much less dependent on the model than the <sup>129</sup>I/<sup>247</sup>Cm ratio (Figure 1). Variations in those three ratios are typically of factors  $\sim 2.5$  to 3 in the WINNET models. Additionally found by some of these models is the <sup>129</sup>I/<sup>127</sup>I ratio of 1.35 derived from the *r*-process abundance of the stable <sup>129</sup>Xe in the Solar System<sup>4</sup>. When considering the PRISM models, which explored a larger set of nuclear inputs, variations are somewhat larger, especially in the case of <sup>247</sup>Cm/<sup>235</sup>U (up to a factor of 10).

All the models show variations in the  $^{129}\text{I}/^{247}\text{Cm}$  ratio of up to three orders of magnitudes (Figure 1, corresponding to Figure S2 of Paper I, but with the PRISM models also included). Of the WINNET models, 13 of them (the nine FMdef models, the three FMs6 Jmhf models, and the FMs6 Jhf4 model) could match the observed  $^{129}\text{I}/^{247}\text{Cm}$  in the ESS. The PRISM models all represent dynamical ejecta and, therefore, provide similar results to the corresponding WINNET models (Bs125, R1010, R1450). As noted above, the PRISM models explore a larger set of nuclear inputs and only one out of those 14 choices (TF\_Mkt) provides a solution for the  $^{129}\text{I}/^{247}\text{Cm}$  ratio in all the four sites.

A quick estimate indicates that self-consistent values of the time elapsed from the last  $r$ -process event (Section 3.1) would result from models with similar values of the  $^{129}\text{I}/^{127}\text{I}$  and  $^{247}\text{Cm}/^{235}\text{U}$  ratios. This is because both the ESS value and the  $K$  values for  $^{129}\text{I}/^{127}\text{I}$  are roughly twice those of  $^{247}\text{Cm}/^{235}\text{U}$ . Therefore, the two differences cancel each other out in the calculation of the ISM ratio needed to derive the time interval of the decay by comparison to the ESS ratio<sup>5</sup>. While there are no models with the same values of the  $^{129}\text{I}/^{127}\text{I}$  and  $^{247}\text{Cm}/^{235}\text{U}$  ratio, when we consider the uncertainties of the  $\tau$  and ESS values, many solutions can be found for a much larger range of relative ratios, as shown in Section 3.1. This is because the time interval of the decay is a function of the natural logarithm of the abundance ratio; therefore, variations in the relative ratios up to a factor of 5 (or even 10) result in a difference, by subtraction, between the time intervals of 1.6 (2.3), which correspond to a percent variation by 30% (50%) only, i.e., well within the uncertainties. For  $^{244}\text{Pu}/^{238}\text{U}$ , instead, it is more difficult to make a quick estimate because of the very different  $\tau$ . In the next section, we evaluate quantitatively, using the WINNET set, the values of the time elapsed between production and incorporation into the first solids in the ESS to verify which models can match the three constraints simultaneously.

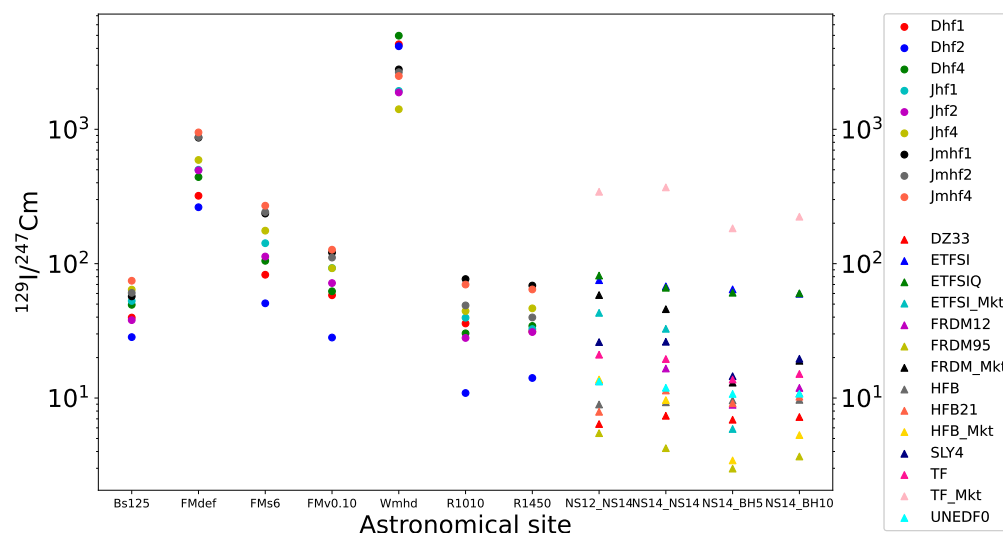


**Figure 1.** Ratios of the  $^{129}\text{I}/^{247}\text{Cm}$  isotopic ratio from all the WINNET (circles) and PRISM (triangles) models, with color as indicated in the box on the right side. The detailed label description can be found in Table 2 and in Paper I. Note that the scale is logarithmic.

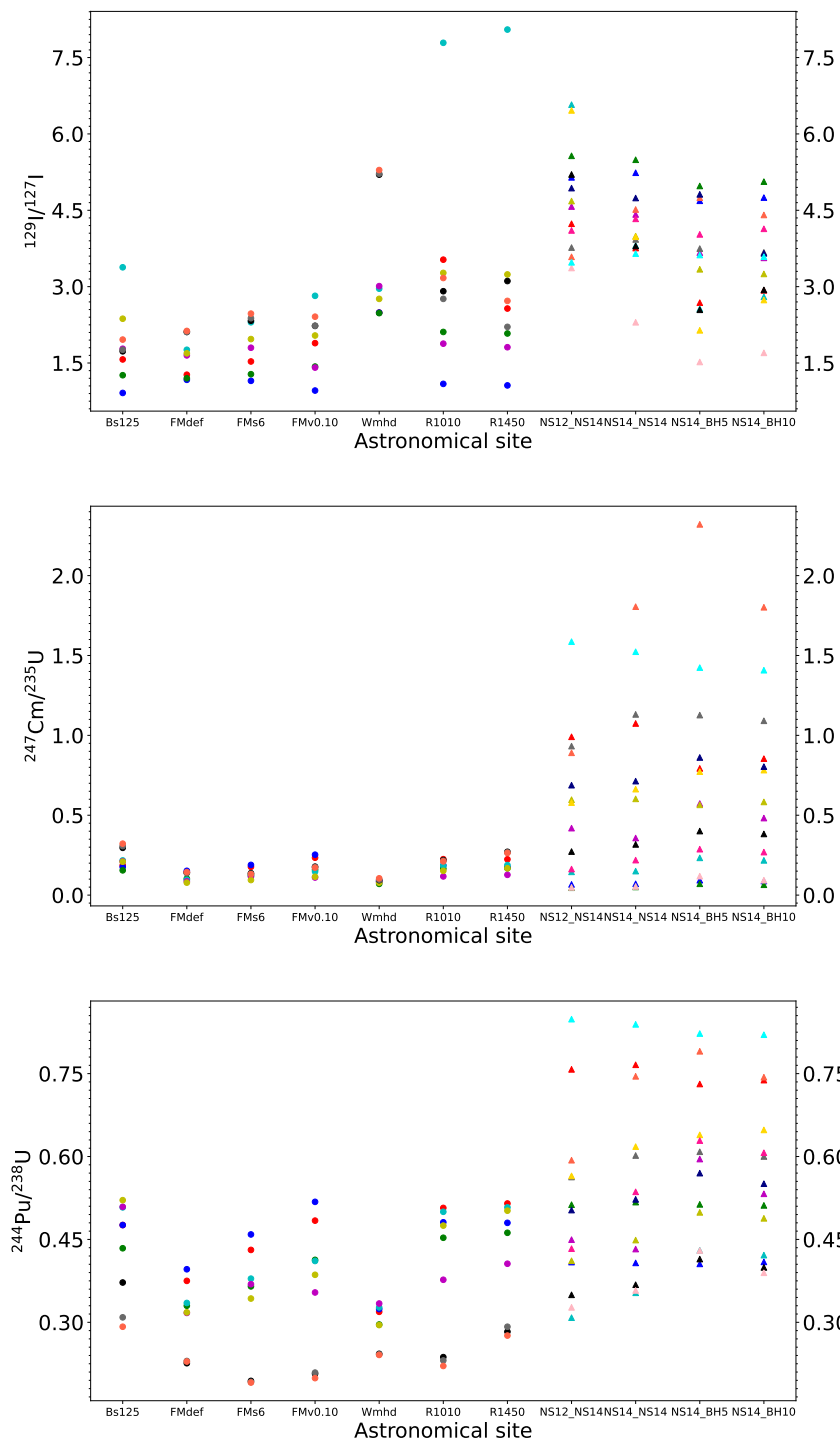


**Figure 2.** Ratios of the abundances of the three SLR of interest to their stable or long-lived isotopes from all the WINNET (circles) and PRISM (triangles) models, with colors as in Figure 1. Note that, differently to Figure 1, all the scales here are linear.

### 3. Galactic Evolution and Origin of the SLRs in the ESS

When considering the ESS data, we need to process the stellar abundances for their recycling within the ISM material from which the Sun formed. Such recycling implies a certain time delay, which is crucial to consider when analysing radioactive isotopes that decay within a given timescale. Côté et al. [29,30] and Yagüe López et al. [11] provided a

methodology and tools to address the evolution in SLR nuclei in the ISM of the Galaxy, and we base our analysis on such works.

First, we need to take into account the uncertainties related to galactic chemical evolution (GCE) itself over the whole lifetime of the Galaxy. These result in a factor  $K$ , by which any ratio predicted by nucleosynthesis calculations involving a stable or long-lived reference isotope needs to be multiplied. This factor takes into account the history of the Galaxy and how it influences the evolution, and therefore the abundance, at the galactic time of the formation of the Sun, of the stable or long-lived isotope that is used as reference for the ESS ratio. The values of  $K$  we calculated from the full GCE models [29] are reported in Table 1 for the three isotopic ratios considered here. Three values are provided: the middle value is the best-fit case and the other two reflect the GCE uncertainties, which provide a minimum and maximum value of the SLR to stable or long-lived isotope ratios. Summarizing Table 1 of [29], the GCE parameters that mostly affect the value of  $K$  are those related to the first and second infall episodes ( $A_1$  and  $A_2$ ) and the star formation efficiency ( $f_{star}$ ). The observational constraints whose uncertainties affect  $K$  the most are the current inflow rate and mass of gas. Due to the feedback between all these quantities, there is not a simple relation with the value of  $K$ . For example, the  $K_{max}$  values are found for the highest values of  $A_2$ ,  $f_{star}$ , and inflow rate, together with the lowest values of  $A_1$  and mass of gas. The reasons for this behaviour are explained in detail in [29].

We found that, if the reference isotope is stable, as in the case of  $^{127}\text{I}$ , the best-fit value of  $K$  is 2.3. When the reference isotope is unstable and long-lived (such as  $^{235,238}\text{U}$ ), the value of  $K$  decreases with the half life of the nucleus because the abundance is affected by a shorter time scale within the full history of the Galaxy. For example, in the case of  $^{235}\text{U}$ , with a half life of  $\sim 1$  Gyr, i.e., roughly ten times shorter than the age of the Galaxy, the  $K$  factor decreases by roughly a factor of two. In the case of  $^{129}\text{I}/^{247}\text{Cm}$ , there are no values of  $K$  to be applied (in other words,  $K$  is always equal to 1) because these two isotopes are both short-lived and insensitive to the past history of our Galaxy. This is one of the several advantages of using such a ratio, as discussed in detail in Paper I.

The other potential problem is that injection of SLR nuclei into the ISM by the stellar objects that produce them is not continuous, because stellar ejection events happen in correspondence to very specific discrete events, e.g., supernova explosions or neutron-star mergers. For stable nuclei, this effect is not significant because their ESS abundances are primarily defined by the total number of events that enriched the pre-solar nebula, rather than by the exact times at which the events occurred. However, for SLR nuclei, this effect can completely control their abundances in the ISM since they freely decay between events. One way to account for this is to consider the average of the interval  $\delta$  between additions to a given parcel of ISM gas from events of a given type, and compare it to the mean-life  $\tau$  of the SLR nuclei produced by this type of events. Therefore, the  $\tau/\delta$  ratio is the crucial parameter to consider, or equivalently  $\tau/\gamma$ , where  $\gamma$  is the time interval between the births of the event progenitors<sup>6</sup>. We do not know a priori the value of  $\tau/\gamma$  for any SLRs and their sources because it depends on uncertain effects such as diffusive transport in the ISM, supernova energetic in carrying material in the ISM, spatial distribution of the events, and distance of the events from the pre-solar ISM parcel of gas (see, e.g., [31] and Wehmeyer et al. in prep). Our approach has therefore been to first develop a general framework and then test its implications and derive its predictions for different values of  $\tau/\gamma$ .

Côté et al. [30] found that, if  $\tau/\gamma > 2$  where  $\gamma$  is the time interval between the births of the event progenitors, then we can treat the injection of SLR from such an event as continuous (hereafter Regime I). We just need to add an uncertainty resulting from the statistical spread of the SLR abundance. If, instead,  $\tau/\gamma < 0.3$ , the most likely scenario is that the ESS abundance of the given SLR came from one last event only, without any memory of the previous events (hereafter Regime III). For values of  $\tau/\gamma$  in-between 0.3 and 2, the SLR abundance carries the memory of a few events (hereafter Regime II). Finally, we note that considering SLR ratios such as the  $^{129}\text{I}/^{247}\text{Cm}$  ratio in the last row of Table 1

significantly reduces the uncertainties resulting from the discrete nature of stellar ejections, especially for cases when the half lives are comparable, as discussed in general in Ref. [11], and in detail for the  $r$ -process SLR in Paper I.

In the following, we use the WINNET abundances to derive more information on the early Solar System and the history of presolar matter from the three  $r$ -process isotopes considered here in different possible scenarios. We remind that the main difference between  $^{129}\text{I}$  and  $^{247}\text{Cm}$ , on the one hand, and  $^{244}\text{Pu}$ , on the other hand, is that the half life of the latter is roughly five times longer than those of the former two. Therefore, the  $\tau/\gamma$  criterion needs to be applied differently, even if all the three isotopes are exclusively produced by  $r$ -process events.

### 3.1. One (Regime III) or Few (Regime II) Events and Time Elapsed from Last Event

In the case of the two  $r$ -process SLR  $^{129}\text{I}$  and  $^{247}\text{Cm}$ , as discussed and presented in detail in Paper I, we can justify statistically the assumption that their abundances in the ESS originated from one last event only, (Regime III), which occurred roughly 100–200 Myr before the formation of the first solids in the Solar System. The criterion  $\tau/\gamma < 0.3$  under which Regime III is valid also for  $^{244}\text{Pu}$  is that  $\gamma$ , or equivalently  $\delta$  in the equation, is greater than 345 Myr. Therefore, possible solutions for this scenario are those for which  $\delta$  is around or larger than this value. To evaluate the ISM  $^{244}\text{Pu}/^{238}\text{U}$  ratio under the assumption that  $^{129}\text{I}$ ,  $^{247}\text{Cm}$ , and  $^{244}\text{Pu}$  in the ESS originated from one event, we then use Equation (S2) of Paper I, as performed in that paper for  $^{129}\text{I}/^{127}\text{I}$  and  $^{247}\text{Cm}/^{235}\text{U}$ , and the values of  $K$  reported in Table 1. Some examples of the calculation of the time from the last event are shown in Figure 3. There, self-consistent solutions are represented by the overlapping areas of the three different colored bands, each representing one of the three SLR isotopes and their uncertainties. The trend with the  $\delta$  of the time elapsed calculated using  $^{244}\text{Pu}$  is steeper than those calculated using the other two isotopes. This is due to its much longer  $\tau$  value and the fact that the time elapsed is a linear function of  $\tau$ .

Figure 3 also shows some examples of possible solutions for Regime II, which corresponds to  $0.3 < \tau/\delta < 2$ , i.e.,  $\delta = 68^7\text{--}345$  Myr. In this case,  $^{244}\text{Pu}$  originated from a few discrete events and the lower the value of  $\delta$ , the larger the number of events. The last event would have contributed only a fraction,  $1 - e^{(-\delta/\tau)}$  (assuming a constant production factor), of the ESS abundance of  $^{244}\text{Pu}$ . Therefore, at the lower limit of Regime II,  $\delta = 68$  Myr, the last event contributed 45% of the ESS abundance of  $^{244}\text{Pu}$ .

Overall, the WINNET set comprises 63 sets of models, and the GCE model provides three values of  $K$  for a total of 189 possibilities. For the first three ratios of Table 1, we found that 92% of the models can provide overlapping solutions: 62 of those with  $K_{\min}$ , 60 of those with  $K_{\text{best}}$ , and 52 of those with  $K_{\max}$ . Therefore, solutions are common, partly thanks to the degree of freedom provided by the relatively free parameter  $\delta$ . Times of the last event are in the range 100–200 Myr as derived in Paper I, this is expected given that the analysis presented here is just an extension of that presented there, to check if the  $^{244}\text{Pu}/^{238}\text{U}$  ratio could also be explained. A new result is that these elapsed times are lower in Regime II than in Regime III, due to the steeper trend with  $\delta$  of those calculated using  $^{244}\text{Pu}$ .

If we include the requirement that the  $^{129}\text{I}/^{247}\text{Cm}$  ratio should be between 254 and  $622^8$ , the number of solutions becomes much more restricted. In fact, the  $^{129}\text{I}/^{247}\text{Cm}$  ratio is a much more stringent constraint because the two isotopes are very far apart in mass and therefore located in very different regions of the nuclide chart. Such relative abundances are more sensitive to the general features of the process and its astrophysical site (such as the amount of free neutrons) as well as the uncertainties in the nuclear model, than the ratios of isotopes that are closer to each other in mass (see Figure 2). As shown in Figure S2 of Paper I, the simulations that produce the best matches to the observations are those dominated by moderately neutron-rich ejecta (in the specific case of the WINNET models, these correspond to the nine FMdef and the three FMs6 Jmhf models).

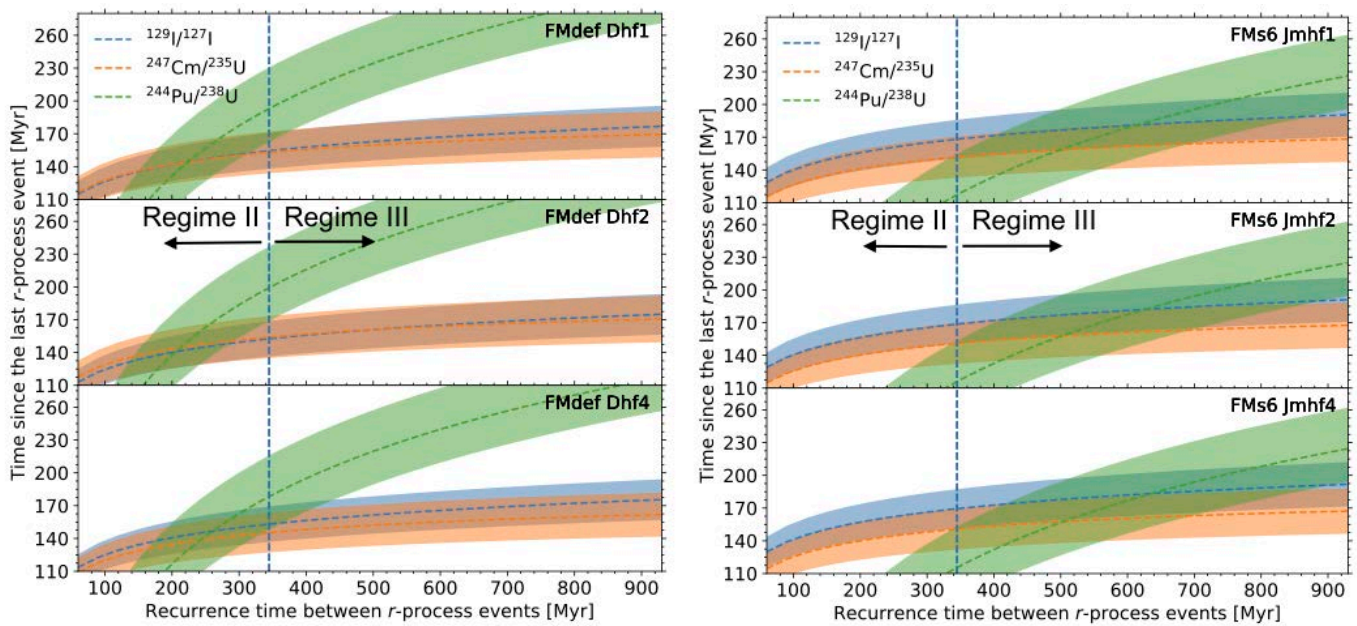


**Figure 3.** Examples of solutions obtained using the WINNET set of yields and  $K_{\text{best}}$  for the time elapsed from the last  $r$ -process event to the formation of the first solids in the ESS that are consistent for all the isotopic ratios of Table 1, except for the right top and middle panels, which correspond to  $^{129}\text{I}/^{247}\text{Cm}$  ratios just outside the required range. The colored dashed lines show the time elapsed as function of the free parameter  $\delta$  derived from each ratio (labels in the top left corner). The dashed blue vertical line represent the  $\delta$  value 345 Myr for which  $\tau_{244}/\delta = 0.3$ , which marks the border between Regimes II and III. Uncertainty bands are a composition of the error distributions around the  $\tau$  and the ESS ratio for each isotope. They are calculated using a Monte-Carlo sampling of such error distributions (using the  $1\sigma$  values and normal distributions, as required). The plotted uncertainty bands are the  $2\sigma$  uncertainty of the Monte-Carlo runs. (Note that these areas are smaller than those shown in Figure S2 of Paper I because there all the different values of  $K$  where included in the bands).

Out of these models, we find that six out of the nine FMdef models (the three Dhf plus the three Jhf cases) and one of the FMs6 model (Jmhf4) can also account for  $^{244}\text{Pu}/^{238}\text{U}$  when using either of the three values of  $K$ , for 21 solutions in total. The main difference between using  $K_{\text{min}}$  and  $K_{\text{best}}$  versus using  $K_{\text{max}}$  is that the former two values provide solutions for  $\delta$  values typical of Regime III, while the latter corresponds to solutions within Regime II. (The FMs6 Jmhf1 and Jmhf2 cases produce  $^{129}\text{I}/^{247}\text{Cm}$  ratios of 236 and 242, respectively, just outside the required range). In summary, more than half (21) of all the 36 possible models that match the  $^{129}\text{I}/^{247}\text{Cm}$  (12 models  $\times$  3 values of  $K = 36$ ) provide a global solution for all the four isotopic ratios.

Finally, we note that, if the ESS  $^{244}\text{Pu}/^{238}\text{U}$  ratio was lower than the value used here, the green shaded area in Figure 3 would shift upwards, for example, by 80 Myr if the ESS ratio was twice as low, due to a longer decay time needed to match the lower ESS value. This would remove most of the Regime III solutions and shift the Regime II solutions to lower values of  $\delta$ .

### 3.2. Steady-State Equilibrium (Regime I) and Isolation Time

In Regime I,  $\tau/\delta$  is  $> 2$ , corresponding to  $\delta < 57.5$  Myr, and  $^{244}\text{Pu}$  evolves in steady-state equilibrium. In this case,  $^{129}\text{I}$  and  $^{247}\text{Cm}$  would be in Regime II; the time elapsed from the last event would decrease with  $\delta$  (as discussed in Section 3.1), and reach roughly 80–130 Myr. The steady-state regime for  $^{129}\text{I}$  and  $^{247}\text{Cm}$  would require, instead, roughly  $\delta < 11$  Myr (for this value of  $\delta$ , at the limit of Regime II, the last event contributed roughly 40% of their ESS abundances). This can be excluded with reasonable confidence because it

is the typical value obtained for core-collapse supernovae, which are much more frequent than the currently accepted  $r$ -process sources.

If  $^{244}\text{Pu}$  was in steady-state equilibrium, then we can use Equation (11) of [1] (where  $K = k + 1$ ) and consider the productions ratios from the  $r$ -process models as a continuous wave of enrichment. In this case, the time interval needed to decay the ISM ratio to its corresponding ESS ratio is an isolation time rather than a time from the last event. This time interval can then be compared to the isolation time obtained from the  $s$ -process isotopes,  $^{107}\text{Pd}$ ,  $^{135}\text{Cs}$ , and  $^{182}\text{Hf}$ , under the assumption of same regime, i.e.,  $\delta < 5 - 6$  Myr for the  $s$ -process events in the Galaxy, which correspond to asymptotic giant branch (AGB) stars of initial mass  $\simeq 2 - 4 M_{\odot}$  [22]. For the three values of  $K$  to be used when studying SLR/stable isotope ratios (i.e., 1.6, 2.3, 5.7, as reported in Table 1 for  $^{129}\text{I}/^{127}\text{I}$ ), the isolation times reported by [22] for the  $s$ -process SLR isotopes are 9–12, 10–16, and 18–26 Myr, respectively. We also need to consider the statistical uncertainty due to stochasticity and discussed in [30]. We can use here the uncertainties reported in Table 3 of [30], for the specific case  $\tau/\gamma = 3.16$  and  $\gamma = 31.6$  Myr, which are close to the maximum uncertainty that would correspond to the case of  $^{244}\text{Pu}$  in this regime. The error is almost symmetric and corresponds to variations in the ISM ratio of +1.16 and  $-0.84$ . These translates into error bars to be applied to each isolation time of +17 and  $-19$  Myr.

In the case of  $K_{\text{max}}$ , no solutions are present because all the isolation times derived from  $^{244}\text{Pu}$  are in the range 61–213 Myr, much higher than the range derived for the  $s$ -process SLR nuclei of 18–26 Myr. This is controlled by the large value of  $K_{\text{max}}$  combined with the long half life of  $^{244}\text{Pu}$ . In the case of  $K_{\text{min}}$  and  $K_{\text{best}}$ , instead, there are 18 and 14 solutions possible, respectively, which have an overlap with the ranges of isolation time derived from the  $s$ -process SLR nuclei. These solutions are all obtained from the models that produce  $^{244}\text{Pu}/^{238}\text{U}$  abundance ratios in the range 0.19–0.34. As shown in Figure 2, these correspond mostly to the WINNET models run with the Jmhf nuclear inputs (out of the total 32 solutions, 23, i.e., 72%, are Jmhf solutions) and the six NS–NS merger PRISM models with SLY4, TF\_Mkt, and UNEDF0. For the other nuclear input choices, instead, only specific astrophysical sites results in  $^{244}\text{Pu}/^{238}\text{U}$  abundance ratios in the required range.

Out of the 12 models that match the three ratios that involve  $^{129}\text{I}$  and  $^{247}\text{Cm}$ , seven of them also provide solutions for the isolation time from  $^{244}\text{Pu}/^{238}\text{U}$  compatible with the  $s$ -process SLR isotopes. However, as mentioned above for the value of  $\delta$  considered here, these two SLR isotopes may have more than one event contributing to their ESS abundances; therefore, such constraints become less strong (see also [31]).

We should also consider the case where  $^{244}\text{Pu}$  is in steady-state, but the  $s$ -process SLRs came from one last event, which requires roughly  $\delta > 30$  Myr for  $s$ -process event in the Galaxy. In this case, the last  $s$ -process event was identified to have occurred at 25 Myr before the formation of the first solids [22], therefore, the isolation time from  $^{244}\text{Pu}/^{238}\text{U}$  is simply constrained to be smaller than this value. Also in this case solutions do not exist with  $K_{\text{max}}$ , while there are 13 and 7 more solutions for  $K_{\text{min}}$  and  $K_{\text{best}}$ , respectively. Most of these solutions overlap as they correspond to the same  $r$ -process models but the different value of  $K$ , therefore, they correspond to the same range of  $^{244}\text{Pu}/^{238}\text{U}$  abundance ratios and nuclear models as reported above. The isolation time from  $^{244}\text{Pu}$  in this case can vary more more freely and there are a few models that given the uncertainties provide values down to zero, which is not a useful constraint. Finally, we note that if the  $s$ -process SLRs originated from a few events (i.e.,  $5 - 6 < \delta < 30$  Myr), then the time from the last event would increase and a few more models could produce an isolation time lower than this value. A more detailed statistical analysis would be needed in this case.

Finally, we note that if the ESS value of the  $^{244}\text{Pu}/^{238}\text{U}$  ratio was twice as high as the value considered here, we would need to add +80 Myr to every isolation time, which would make it impossible to find a solution consistent with the origin of the  $s$ -process SLR isotopes.

#### 4. Summary and Conclusions

We presented and analysed the relative production of the short-lived and long-lived  $r$ -process isotopes  $^{129}\text{I}$ ,  $^{235}\text{U}$ ,  $^{238}\text{U}$ ,  $^{244}\text{Pu}$ , and  $^{247}\text{Cm}$  and the stable  $^{127}\text{I}$  in a large set of 119  $r$ -process models from two different sets calculated with the WINNET and PRISM frameworks. We then investigated if it is possible to find solutions for the origin of the ESS abundance of  $^{244}\text{Pu}$  that provide production at the source and time intervals (either from the last event or from the time of the isolation, depending on the  $\tau/\delta$  regime) compatible to those of the other  $r$ -process and  $s$ -process SLR isotopes. A summary of the different possibilities, solutions, and derived time intervals are shown in Table 3. In brief:

**Table 3.** Summary of the different regimes combinations for the different SLRs, their corresponding  $\delta$  values in Myr ( $\delta_r$  and  $\delta_s$ , for the  $r$ - and  $s$ -process events, respectively),  $r$ -process model solutions, and elapsed time ( $t_{e,r}$  and  $t_{e,s}$ , for the last  $r$ - and  $s$ -process event, respectively) or isolation time ( $t_i$ ) in Myr. Notes: <sup>a</sup> For all the four ratios in Table 1:  $6 = \text{FMdef}(3\times\text{Dhf},3\times\text{Jhf}) + \text{FMs6Jmhf4}$ , all valid for each of the three values of  $K$ . We did not check the PRISM models for these regimes. <sup>b</sup> Of which 23 have Jmhf nuclear input. <sup>c</sup> The two NS–NS merger models with the three nuclear inputs: SLY4, TF\_Mkt, and UNEDF0.

Regime	$\delta$ (Myr)	Solutions	Times (Myr)
III for $^{129}\text{I}$ , $^{247}\text{Cm}$ , and $^{244}\text{Pu}$ III for $^{129}\text{I}$ and $^{247}\text{Cm}$ and II for $^{244}\text{Pu}$	$\delta_r > 345$ $68 < \delta_r < 345$	7 WINNET <sup>a</sup>	$t_{e,r} \simeq 100\text{--}200$
II for $^{129}\text{I}$ and $^{247}\text{Cm}$ and I for $^{244}\text{Pu}$ , $^{107}\text{Pd}$ , and $^{182}\text{Hf}$ OR III for $^{107}\text{Pd}$ and $^{182}\text{Hf}$	$11 < \delta_r < 68$ , $\delta_s < 5$ $11 < \delta_r < 68$ , $\delta_s > 30$	32 WINNET <sup>b</sup> , 6 PRISM <sup>c</sup> , 0 for $K_{\text{max}}$ 20 more than above	$t_{e,r} \simeq 80\text{--}130$ , $t_i \simeq 9\text{--}16$ $t_{e,s} \simeq 25$ , $t_i > 0$

1. In Section 3.1 (top section of Table 3), we considered Regimes II and III for  $^{244}\text{Pu}$ , corresponding to  $\delta > 68$  Myr and Regime III for  $^{129}\text{I}$  and  $^{247}\text{Cm}$ . More than half of the WINNET models that were already shown to reproduce the three ratios that involve  $^{129}\text{I}$  and  $^{247}\text{Cm}$  in Paper I, also provide a self-consistent solution for  $^{244}\text{Pu}$ . These models all correspond to the NS–NS merger disk cases dominated by moderately neutron-rich ejecta.
2. In Section 3.2 (bottom section of Table 3), we considered Regime I for  $^{244}\text{Pu}$ , i.e.,  $\delta < 68$  Myr, where this SLR reaches a steady-state value in the ISM. It is also possible to find a significant number of  $r$ -process models (mostly corresponding to the Jmhf nuclear input) that provide solutions for the ESS  $^{244}\text{Pu}$  abundance compatible to those of the SLR isotopes produced also by the  $s$  process:  $^{107}\text{Pd}$  and  $^{182}\text{Hf}$  (and the current ESS upper limit of  $^{135}\text{Cs}$ ). However, no solutions exist in Regime I for  $^{244}\text{Pu}$  if the ESS value of  $^{244}\text{Pu}$  was twice as high as the value used here or if the Milky Way model was represented by  $K_{\text{max}}$ .

We cannot determine if the solution to the origin of  $^{244}\text{Pu}$  in the ESS is 1. or 2. above, and which implications on the timescales are valid, since we still do not know how far material from  $r$ -process sources can travel, and, therefore, how many parcels of the ISM are affected by each of these events and the value of  $\delta$ . Although we note that recent hydrodynamical models aimed at calculating how far material travels after being ejected by a hypernova predict relatively short distances [32], which would support large  $\delta$  values for the  $r$ -process events. In any case, we have established that within Point 1., WINNET solutions within the NS–NS disk ejecta favour the Dhf and Jhf nuclear models. Within Point 2., all solutions exclude the case of a Milky Way Galaxy with  $K_{\text{max}}$ , therefore restricting the isolation time to 9–16 Myr (if  $^{107}\text{Pd}$  and  $^{182}\text{Hf}$  are also in Regime I), still supporting the hypothesis that the Sun was born in a massive, long-living molecular cloud. We can also conclude that a much lower value of the  $^{244}\text{Pu}/^{238}\text{U}$  ratio in the ESS than that reported in Table 1 would be impossible to reconcile within Regime I, and would therefore support

Regimes II and III. New, future experiments and analysis are needed to confirm the ESS  $^{244}\text{Pu}/^{238}\text{U}$  ratio.

**Supplementary Materials:** The following supporting information can be downloaded at: <https://www.mdpi.com/article/10.3390/universe8070343/s1>, Table S1: WINNET-abundances.txt; Table S2: PRISM-ratios.txt.

**Author Contributions:** All the authors have contributed to the conceptualization, methodology, software, validation, formal analysis, and investigation. The original draft was prepared by M.L. and M.P. (Marco Pignatari) with Figure 1 contributed by B.S. and Figure 2 by A.Y.L., B.S., B.C., M.P. (Mária Pető), N.V., B.W. and M.P. (Marco Pignatari) contributed to the methodology, as well as the review and editing of the paper. M.L. contributed to the supervision, project administration, and funding acquisition for the project. All authors have read and agreed to the published version of the manuscript.

**Funding:** This research was funded by ERC via CoG-2016 RADIOSTAR (Grant Agreement 724560). The work of A.Y.L. was supported by the US Department of Energy through the Los Alamos National Laboratory. Los Alamos National Laboratory is operated by Triad National Security, LLC, for the National Nuclear Security Administration of U.S. Department of Energy (Contract No. 89233218CNA000001). B.C. acknowledges support of the National Science Foundation (USA) under grant No. PHY-1430152 (JINA Center for the Evolution of the Elements).

**Institutional Review Board Statement:** Not applicable.

**Informed Consent Statement:** Not applicable.

**Data Availability Statement:** Not applicable.

**Acknowledgments:** We thank Marius Eichler, Almudena Arcones, and Thomas Raucher for providing us with the WINNET models and their results of *r*-process nucleosynthesis. We thank Matthew Mumpower, Trevor Spouse, and Rebecca Surman for their contributions to the PRISM models. We also thank Jamie Gilmour for discussion on the ESS data. MP acknowledges support of NuGrid from NSF grant PHY-1430152 (JINA Center for the Evolution of the Elements) and STFC (through the University of Hull's Consolidated Grant ST/R000840/1), and access to VIPER, the University of Hull High Performance Computing Facility. MP acknowledges the support from the "Lendület-2014" Programme of the Hungarian Academy of Sciences (Hungary). We thank the ChETEC COST Action (CA16117), supported by COST (European Cooperation in Science and Technology), and the ChETEC-INFRA project funded from the European Union's Horizon 2020 research and innovation programme (grant agreement No 101008324), and the IReNA network supported by NSF AccelNet.

**Conflicts of Interest:** The authors declare no conflict of interest. The funders had no role in the design of the study; in the collection, analyses, or interpretation of data; in the writing of the manuscript, or in the decision to publish the results.

## Abbreviations

The following abbreviations are used in this manuscript:

ESS	early Solar System
GCE	galactic chemical evolution
ISM	interstellar medium
NSM	neutron star merger
<i>r</i> process	<i>rapid</i> neutron-capture process
<i>s</i> process	<i>slow</i> neutron-capture process
SLR	short-lived radioactive

## Notes

- The mean-life  $\tau_{ratio}$  of the  $^{129}\text{I}/^{247}\text{Cm}$  ratio given in the table was obtained by Monte Carlo sampling of the uncertainties on the mean lives of the two isotopes,  $\tau_{129}$  and  $\tau_{247}$ , which are 5% and 6%, respectively, at  $2\sigma$  (for comparison, the uncertainty for  $^{244}\text{Pu}$  is 2%) within the usual formula:  $\tau_{129} \times \tau_{247} / (\tau_{129} - \tau_{247})$ . Using the recommended values,  $\tau_{ratio}$  would be equal to 2449 Myr, however, sampling of the uncertainties produces a lower value most of the time because the uncertainties make  $\tau_{129}$  and  $\tau_{247}$  move away from each other, and therefore their difference, at denominator in the formula above, increases. In general, it would

be extremely useful if the half lives of  $^{129}\text{I}$  and  $^{247}\text{Cm}$  could be measured with higher precision than currently available. A more detailed statistical analysis should also be carried out considering that the peak value reported in the table is probably not the best statistical choice due to the exponential behaviour of the decay. In fact, although  $\tau \sim 270$  Myr is the most common value, when  $\tau \gtrsim 1000$  Myr abundances do not vary much anymore within the time scales, roughly  $<200$  Myr are of interest for the ESS (discussed in Section 3). Therefore, a more statistically significant value may be higher than the peak value reported in the table, probably around 900 Myr. For the other ratios, the values of the mean lives at numerator and denominator in the equation above are so different that  $\tau_{\text{ratio}}$  is always within 2% of the  $\tau$  of the short-lived isotope. A statistical analysis of the uncertainties would not affect those values, although we will analyse statistically the impact of the uncertainties on all the mean lives when we derive timescales in Section 3.

<sup>2</sup> <https://zenodo.org/record/4446099#.YgKVxWAO-mk> (accessed on 15 June 2022).

<sup>3</sup> <https://zenodo.org/record/4456126#.YgKV0GAO-mk> (accessed on 15 June 2022).

<sup>4</sup> This is calculated using the residual method, where the  $r$ -process abundance is the total solar abundance of  $^{129}\text{Xe}$  minus the predicted  $s$ -process abundance. This method cannot be applied to  $^{247}\text{Cm}$  and  $^{244}\text{Pu}$  as these isotopes do not have one daughter stable nucleus produced exclusively by their decay.

<sup>5</sup> When we also consider the difference due to fact that while  $^{127}\text{I}$  is stable,  $^{235}\text{U}$  will also decay. For time intervals of the order of 100–200 Myr, this corresponds to a small effect on the  $^{247}\text{Cm}/^{235}\text{U}$  ratio of roughly 10–20%.

<sup>6</sup> Since  $\gamma \simeq \delta$  (see detailed discussion in [30]) for our purposes here  $\gamma$  will be considered equivalent to  $\delta$ .

<sup>7</sup> This lower limit is defined such that  $\tau/\delta < 0.3$  for  $^{129}\text{I}$  and  $^{247}\text{Cm}$ , but it is close to the 57.5 Myr value defined by  $\tau/\delta > 2$  for  $^{244}\text{Pu}$ .

<sup>8</sup> Note that the evaluation of the ESS ratio of  $^{129}\text{I}/^{247}\text{Cm}$  depends on the time from the last event itself, given that its  $\tau_{\text{ratio}}$  is variable due to the uncertainties in  $\tau_{129}$  and  $\tau_{247}$ , as discussed in Section 1. The ESS values reported in Table 1 and used here were calculated assuming a time from last event in the range 100–200 Myr and composing all the uncertainties, as discussed in detail in the supplementary material of Paper I. A more precise analysis would instead use the range of times from the last event for each model solution to derive the range of corresponding ESS  $^{129}\text{I}/^{247}\text{Cm}$  ratios, and find if the model matches such a specific range. However, given that, as noted above, most solutions provide times in the 100–200 Myr range, this more accurate treatment would not change our results.

## References

- Lugaro, M.; Ott, U.; Kereszturi, Á. Radioactive nuclei from cosmochronology to habitability. *Progr. Part. Nucl. Phys.* **2018**, *102*, 1–47. [CrossRef]
- Wallner, A.; Faestermann, T.; Feige, J.; Feldstein, C.; Knie, K.; Korschinek, G.; Kutschera, W.; Ofan, A.; Paul, M.; Quinto, F.; et al. Abundance of live  $^{244}\text{Pu}$  in deep-sea reservoirs on Earth points to rarity of actinide nucleosynthesis. *Nat. Commun.* **2015**, *6*, 5956. [CrossRef]
- Wallner, A.; Froehlich, M.B.; Hotchkis, M.A.C.; Kinoshita, N.; Paul, M.; Martschini, M.; Pavetich, S.; Tims, S.G.; Kivel, N.; Schumann, D.; et al.  $^{60}\text{Fe}$  and  $^{244}\text{Pu}$  deposited on Earth constrain the  $r$ -process yields of recent nearby supernovae. *Science* **2021**, *372*, 742–745. [CrossRef]
- Ratzel, U.; Arlandini, C.; Käppeler, F.; Couture, A.; Wiescher, M.; Reifarth, R.; Gallino, R.; Mengoni, A.; Travaglio, C. Nucleosynthesis at the termination point of the  $s$  process. *Phys. Rev. C* **2004**, *70*, 065803. [CrossRef]
- Cowan, J.J.; Sneden, C.; Lawler, J.E.; Aprahamian, A.; Wiescher, M.; Langanke, K.; Martínez-Pinedo, G.; Thielemann, F.K. Origin of the heaviest elements: The rapid neutron-capture process. *Rev. Mod. Phys.* **2021**, *93*, 015002. [CrossRef]
- Lugaro, M.; Heger, A.; Osrin, D.; Goriely, S.; Zuber, K.; Karakas, A.I.; Gibson, B.K.; Doherty, C.L.; Lattanzio, J.C.; Ott, U. Stellar origin of the  $^{182}\text{Hf}$  cosmochronometer and the presolar history of solar system matter. *Science* **2014**, *345*, 650–653. [CrossRef]
- Hotokezaka, K.; Piran, T.; Paul, M. Short-lived  $^{244}\text{Pu}$  points to compact binary mergers as sites for heavy  $r$ -process nucleosynthesis. *Nat. Phys.* **2015**, *11*, 1042–1044. [CrossRef]
- Côté, B.; Eichler, M.; Yagüe López, A.; Vassh, N.; Mumpower, M.R.; Világos, B.; Soós, B.; Arcones, A.; Sprouse, T.M.; Surman, R.; et al.  $^{129}\text{I}$  and  $^{247}\text{Cm}$  in meteorites constrain the last astrophysical source of solar  $r$ -process elements. *Science* **2021**, *371*, 945–948. [CrossRef]
- Wang, X.; Clark, A.M.; Ellis, J.; Ertel, A.F.; Fields, B.D.; Fry, B.J.; Liu, Z.; Miller, J.A.; Surman, R.  $r$ -Process Radioisotopes from Near-Earth Supernovae and Kilonovae. *Astrophys. J.* **2021**, *923*, 219. [CrossRef]
- Wang, X.; Clark, A.M.; Ellis, J.; Ertel, A.F.; Fields, B.D.; Fry, B.J.; Liu, Z.; Miller, J.A.; Surman, R. Future radioisotope measurements to clarify the origin of deep-ocean  $^{244}\text{Pu}$ . *arXiv* **2021**, arXiv:astro-ph.HE/2112.09607.
- Yagüe López, A.; Côté, B.; Lugaro, M. Monte Carlo Investigation of the Ratios of Short-lived Radioactive Isotopes in the Interstellar Medium. *Astrophys. J.* **2021**, *915*, 128. [CrossRef]
- Gilmour, J.D.; Pravdivtseva, O.V.; Busfield, A.; Hohenberg, C.M. The I-Xe chronometer and the early solar system. *Meteorit. Planet. Sci.* **2006**, *41*, 19–31. [CrossRef]
- Tissot, F.L.H.; Dauphas, N.; Grossman, L. Origin of uranium isotope variations in early solar nebula condensates. *Sci. Adv.* **2016**, *2*, e1501400. [CrossRef]

14. Wasserburg, G.J.; Huneke, J.C.; Burnett, D.S. Correlation Between Fission Tracks and Fission-Type Xenon from an Extinct Radioactivity. *Phys. Rev. Lett.* **1969**, *22*, 1198–1201. [[CrossRef](#)]
15. Marti, K.; Lugmair, G.W.; Scheinin, N.B. Sm-Nd-Pu Systematics in the Early Solar System. In Proceedings of the Lunar and Planetary Science Conference, Houston, TX, USA, 14–18 March 1977; Volume 8, p. 619. Available online: <https://articles.adsabs.harvard.edu/full/1977LPL....8..619M> (accessed on 15 June 2022).
16. Podosek, F.A.; Lewis, R.S.  $^{129}\text{I}$  and  $^{244}\text{Pu}$  abundances in white inclusions of the Allende meteorite. *Earth Planet. Sci. Lett.* **1972**, *15*, 101–109. [[CrossRef](#)]
17. Lugmair, G.W.; Marti, K. Sm sbnd Nd sbnd Pu timepieces in the Angra dos Reis meteorite. *Earth Planet. Sci. Lett.* **1977**, *35*, 273–284. [[CrossRef](#)]
18. Shukolyukov, A.; Begemann, F. Pu-Xe dating of eucrites. *Geochim. Cosmochim. Acta* **1996**, *60*, 2453–2471. [[CrossRef](#)]
19. Hudson, G.B.; Kennedy, B.M.; Podosek, F.A.; Hohenberg, C.M. The early solar system abundance of Pu-244 as inferred from the St. Severin chondrite. In *Lunar and Planetary Science Conference Proceedings*; Ryder, G., Sharpton, V.L., Eds.; Cambridge University Press: Houston, TX, USA, 1989; Volume 19, pp. 547–557.
20. Connelly, J.N.; Bizzarro, M.; Krot, A.N.; Nordlund, A.; Wielandt, D.; Ivanova, M.A. The Absolute Chronology and Thermal Processing of Solids in the Solar Protoplanetary Disk. *Science* **2012**, *338*, 651–655. [[CrossRef](#)]
21. Turner, G.; Busfield, A.; Crowther, S.A.; Harrison, M.; Mojzsis, S.J.; Gilmour, J. Pu Xe, U Xe, U Pb chronology and isotope systematics of ancient zircons from Western Australia. *Earth Planet. Sci. Lett.* **2007**, *261*, 491–499. [[CrossRef](#)]
22. Trueman, T.C.L.; Côté, B.; Yagüe López, A.; den Hartogh, J.; Pignatari, M.; Soós, B.; Karakas, A.I.; Lugaro, M. Galactic Chemical Evolution of Radioactive Isotopes with an s-process Contribution. *Astrophys. J.* **2022**, *924*, 10. [[CrossRef](#)]
23. Eichler, M.; Arcones, A. Detailed Abundances Based on Different Nuclear Physics for Theoretical R-Process Scenarios. 2021. Available online: <https://zenodo.org/record/4446099#.YrKSFSdBxPY> (accessed on 15 June 2022).
24. Winteler, C.; Käppeli, R.; Perego, A.; Arcones, A.; Vasset, N.; Nishimura, N.; Liebendörfer, M.; Thielemann, F.K. Magnetorotationally Driven Supernovae as the Origin of Early Galaxy r-process Elements? *Astrophys. J. Lett.* **2012**, *750*, L22. [[CrossRef](#)]
25. Vassh, N.; Mumpower, M.R.; Sprouse, T.M.; Surman, R. r-Process Abundances in Neutron-Rich Merger Ejecta Given Different Theoretical Nuclear Physics Inputs. 2021. Available online: <https://zenodo.org/record/4456126#.YrKSuCdBxPY> (accessed on 15 June 2022).
26. Mumpower, M.R.; Kawano, T.; Sprouse, T.M.; Vassh, N.; Holmbeck, E.M.; Surman, R.; Möller, P.  $\beta$ -delayed Fission in r-process Nucleosynthesis. *Astrophys. J.* **2018**, *869*, 14. [[CrossRef](#)]
27. Eichler, M.; Sayar, W.; Arcones, A.; Rauscher, T. Probing the Production of Actinides under Different r-process Conditions. *Astrophys. J.* **2019**, *879*, 47. [[CrossRef](#)]
28. Freiburghaus, C.; Rosswog, S.; Thielemann, F.K. R-Process in Neutron Star Mergers. *Astrophys. J.* **1999**, *525*, L121–L124. [[CrossRef](#)]
29. Côté, B.; Lugaro, M.; Reifarth, R.; Pignatari, M.; Világos, B.; Yagüe, A.; Gibson, B.K. Galactic Chemical Evolution of Radioactive Isotopes. *Astrophys. J.* **2019**, *878*, 156. [[CrossRef](#)]
30. Côté, B.; Yagüe, A.; Világos, B.; Lugaro, M. Stochastic Chemical Evolution of Radioactive Isotopes with a Monte Carlo Approach. *Astrophys. J.* **2019**, *887*, 213. [[CrossRef](#)]
31. Banerjee, P.; Wu, M.R.; Jeena, S.K. Constraints on R-process nucleosynthesis from  $^{129}\text{I}$  and  $^{247}\text{Cm}$  in the early solar system. *Mon. Not. R. Astron. Soc.* **2022**, *512*, 4948–4960. [[CrossRef](#)]
32. Amend, B.; Zrake, J.; Hartmann, D.H. R-process Rain from Binary Neutron Star Mergers in the Galactic Halo. *arXiv* **2022**, arXiv:2205.03913.